FePt nanoalloys anchored reduced graphene oxide as high-performance electrocatalysts for formic acid and methanol oxidation

Jinxue Guo, Yanfang Sun, Xiao Zhang, Lin Tang, Hongtian Liu

PII: S0925-8388(14)00665-3
DOI: http://dx.doi.org/10.1016/j.jallcom.2014.03.077
Reference: JALCOM 30848

To appear in:

Received Date: 6 January 2014
Revised Date: 10 March 2014
Accepted Date: 12 March 2014

Please cite this article as: J. Guo, Y. Sun, X. Zhang, L. Tang, H. Liu, FePt nanoalloys anchored reduced graphene oxide as high-performance electrocatalysts for formic acid and methanol oxidation, (2014), doi: http://dx.doi.org/10.1016/j.jallcom.2014.03.077

FePt nanoalloys anchored reduced graphene oxide as high-performance electrocatalysts for formic acid and methanol oxidation

Jinxue Guo, Yanfang Sun, Xiao Zhang*, Lin Tang, Hongtian Liu

Key Laboratory of Sensor Analysis of Tumor Marker (Ministry of Education), Lab of Advanced Energy Materials Chemistry, College of Chemistry and Molecular Engineering, Qingdao University of Science and Technology, Qingdao 266042, China

ABSTRACT

Reduced graphene oxide (RGO) supported FePt alloy nanoparticles are synthesized as high-performance electrocatalysts for methanol and formic acid (FA) oxidation. The microstructure, composition and morphology of the sample are systematically characterized with X-ray diffraction (XRD), fourier transform infrared spectroscopy (FT-IR), scanning electron microscope (SEM), transmission electron microscope (TEM), energy dispersive spectroscopy (EDS) and Raman spectroscopy. The electrocatalytic tests reveal that, in comparison with pure Pt nanoparticles supported on RGO sheets, the FePt nanoalloys anchored RGO sheets deliver remarkably enhanced electrocatalytic performance on FA/methanol oxidation, improved tolerance to CO poisoning, and superior catalytic durability.

Keywords: nanostructured materials; catalyst; composite materials; fuel cells

1. Introduction

* Corresponding author. Tel.: +86 532 84022681; Fax: +86 532 84023927.

E-mail address: zhx1213@126.com (X. Zhang).

In recent decades, fuel cells have been investigated intensively as the sustainable energy source because they can electrochemically convert hydrogen into water or methanol/formic acid (FA)/ethanol into water and carbon dioxide to generate electricity [1]. Among different types of electrocatalysts, platinum (Pt) has been demonstrated as the most efficient catalyst for low-temperature fuel cells [2-4]. Unfortunately, the prohibitive cost of Pt catalyst as well as the finite utilization efficiency has hampered its widespread commercialization. To overcome these obstacles, recent efforts have been focused on decreasing the Pt content in fuel cell catalysts through the effective strategy of alloying Pt with other inexpensive metals, such as Fe, Co, Ni, Cu, Ti, Pb, Zn, Cd, Hg, and Sn [5-19]. Xu et al. have prepared Pt-Cu nanocube catalysts with good catalytic stability for FA oxidation through a colloidal approach [11]. Habibi and co-workers have prepared Pt-Sn bimetallic electrocatalyst which shows good catalytic activity for FA oxidation via the electrochemical deposition process [16]. Pt-Pb hollow sphere has been synthesized by Zhao et al. for FA electrooxidation [19]. Specially, the preparation and application of FePt alloys are on the focus. For instance, Guo et al. have deposited FePt nanoparticles on reduced graphene oxide (RGO) through solution-phase self-assembly for oxygen reduction reaction [13]. Wei and co-workers have prepared FePt-graphene nanohybrids for ethanol and methanol oxidation using $NaBH_4$ as reducing agent [14]. Ji et al. have prepared RGO supported FePt alloy for methanol oxidation using hydrazine hydrate as reducing agent [18]. Nevertheless, it is still a great challenge to synthesize high-quality FePt bimetallic nanoalloys as high-performance electrocatalyst through a simple approach.

In this paper, we report a facile and efficient two-step approach to prepare FePt alloy nanoparticles anchored on RGO composites (FePt/RGO) as a cost sustainable electrocatalyst for fuel cell applications. RGO sheets are used as the substrate due to its high electrical conductivity, 2-dimensional mechanical flexibility, huge surface area, and good chemical stability [20,21]. The electrochemical tests reveal that, the obtained FePt/RGO catalysts exhibit enhanced electrocatalytic activity on FA/methanol oxidation, improved tolerance to CO poison, and better catalytic stability than that of Pt nanoparticles supported on RGO composites (Pt/RGO).

2. Experimental

2.1 Materials preparation

Natural graphite is oxidized according to a modified Hummers method [22], and the detailed process can be presented as follows: Graphite powder (2 g) and $NaNO_3$ (1 g) are added into 50 mL of concentrated H_2SO_4 (98%) with vigorous stirring. The mixture is kept below 5 ^oC in an ice bath and stirred for 30 min. Then 0.3 g $KMnO_4$ is added into the above mixture and stirred for 30 min, the temperature is kept below 10 ^oC. Subsequently, 7 g of $KMnO_4$ is added gradually within 1 h under stirring, in order to prevent the temperature of the mixture from exceeding 20 ^oC. After the ice bath is removed, the mixture is stirred at 35 ± 3 ^oC for 2 h and a brown dispersion solution is obtained. Then 90 mL of distilled water is poured into the above dispersion, and the temperature is kept above 90 ^oC for 15 min. The reaction is terminated by adding 55 mL of distilled water and 10 mL of 30% H_2O_2 solution. The resultant light yellow

dispersion is filtered, washed with 1 M HCl aqueous solution two times, and then washed with distilled water. The obtained products are exfoliated with ultrasonication in water for more than 1 h. The resultant homogeneous brown-black GO dispersion is about 10 mg ml^{-1} and remains stable for months.

The synthesis of FePt/RGO consists of two steps: Firstly, 24 mg of $K_4Fe(CN)_6 \cdot 3H_2O$ is dissolved in 24 mL deionized water. The solution is poured into 6 mL GO solution (10 mg mL^{-1}) under vigorous stirring. After ultrasonic for 30 min, the mixed solution is transferred into a 40 mL autoclave and maintained at 180 ^oC for 24 h. The products are harvested and then washed with absolute ethanol and water in turn before they are dried at 60 ^oC for 12 h in vacuum. In the second step, 60 mg of the hydrothermal products are dispersed into 60 mL $H_2PtCl_6 \cdot 3H_2O$ solution (0.5 mg mL^{-1}). The dispersion is under ultrasonic irradiation for 30 min and then evaporated at 80 ^oC under vigorous stirring. After dried, the black powders are loaded into a tube furnace and sintered at 120 ^oC for 2 h in H_2/Ar (volume ratio of 5/95) atmosphere with a heating rate of 1 ^oC min^{-1} to prepare the final products of FePt/RGO. For comparison, 6 mL GO solution (10 mg mL^{-1}) is directly mixed with 60 mL $H_2PtCl_6 \cdot 3H_2O$ solution (0.5 mg mL^{-1}). After ultrasonic for 30 min and vigorous stirring at 80 ^oC, Pt/RGO is obtained by calcination at 120 ^oC in H_2/Ar atmosphere.

2.2 Characterizations

The crystal structure and composition of the sample are determined with powder X-ray powder diffraction (XRD, Philips X'-pert X-ray diffractometer). Scanning

electron microscope (SEM) and energy dispersive spectroscopy (EDS) are obtained with a JEOL JSM-7500F. Transmission electron microscope (TEM) is recorded on a JEOL, JEM-2100. Fourier transform infrared (FTIR) spectra are performed using a Nicolet Magna-IR750. Raman spectroscopy is measured on a confocal microprobe Raman system (LabRam-010, 632 nm as the excitation source).

2.3 Electrochemical measurements

All the electrochemical measurements are carried out on CHI600D (CH Instruments, Shanghai, China) with a conventional three-electrode cell at 25 ˚C. Modified glassy carbon electrode (GCE), a plate wire, and a saturated calomel electrode (SCE) are used as the working, counter, and reference electrode, respectively. To fabricate a working electrode, homogeneous catalyst ink is prepared by ultrasonically dispersing the mixture of 2 mg catalyst, 0.5 mL Nafion solution (0.05wt.%), and 0.5 mL ethanol. The catalyst ink (3 μL) is casted on the pretreated GCE surface, leading to a catalyst loading of 6 μg. After the solvent evaporates, the modified electrode is obtained as the working electrode for all the electrochemical tests. The electrocatalytic activities of the Pt/RGO and FePt/RGO catalysts for oxidation of FA/methanol are measured in 0.5 M H_2SO_4 solution containing 1 M HCOOH/ 0.5 M CH_3OH by cyclic voltammograms (CV) from -0.2 V to 1.2 V at a scan rate of 50 mV s^{-1}. Choronoamperometrc curves are obtained at a fixed potential of 0.3 V (FA oxidation) and 0.6 V (methanol oxidation) for 10 min. The electrolyte solutions are deaerated by bubbling with N_2 for 15 min prior to electrochemical tests.

3. Results and discussion

3.1 Formation of FePt-RGO

The XRD patterns are used to determine the composition and crystal structure of the as-prepared GO, Pt/RGO nanocomposites and FePt/RGO nanocomposites. As is shown in Fig. 1a, the sharp diffraction peak at 2θ of ~9.3°corresponding to the (001) reflection is observed in the XRD pattern of GO, indicating the successful transformation of natural graphite into GO. As for the Pt/RGO and FePt/RGO nanocomposites, the (001) peak is absent, while a broad peak located at 2θ of ~25° appears, which can be assigned to the characteristic short-range order of stacked graphene sheets [18,23]. This result suggests that GO has been reduced into RGO in the composites. Moreover, three other peaks at 40°, 46°, and 68° are observed in both Pt/RGO and FePt/RGO nanocomposites, which can be well indexed to the (111), (200), and (220) planes of face-centered cubic structure of Pt or FePt nanoalloys (JCPDS card no. 04-0802). In the XRD pattern of FePt/RGO nanocomposites, no other impurity peaks according to metallic Fe or its oxides are detected, indicating its high phase purity. It is well accepted that, the nanoparticle size can be approximately calculated from the widths of peaks using Debye-Scherrer equation: $d = K\lambda/\beta cos\theta$, where d is the average particle size, K is Debye-Scherrer constant (0.89), λ is the X-ray wavelength, β is the full-width half maximum (FWHM) and θ is the angle of diffraction. The mean particle size of FePt alloy nanoparticles is evaluated to be ~5.9 nm from the strongest (111) peak, which is smaller than the Pt nanoparticles of ~7.3 nm. Interestingly, the characteristic peaks

corresponding to FePt nanoalloys shift slightly to higher 2θ values compared with that of Pt nanoparticles in Pt/RGO. In order to observe more clearly, the magnified diffraction intensity of the strongest peak of (111) plane is presented in Fig. 1b. It is shown that the 2θ value of (111) plane for FePt nanoalloys is obviously higher than that of Pt nanocrystals, which can be attributed to the contraction of the lattice constants, confirming the successfully alloy formation between Fe and Pt.

The FTIR spectra of GO and FePt/RGO nanocomposites are measured. As shown in Fig. 2, the FTIR spectrum of GO reveals the successful oxidation of graphite [18,24]. The absorption bands centered at 3400 and 1400 cm^{-1} are corresponding to O-H (carboxyl). The bands of 1720 cm^{-1} can be assigned to the stretching vibration of C=O (carboxyl). The bands located at 1225 and 1050 cm^{-1} can be attributed to C-O (epoxy) and C-O (carboxyl or alkoxy), respectively. The vibration of C-OH (hydroxyl) is observed at 1625 cm^{-1}. The peak at 1580 cm^{-1} is corresponding to the characteristic skeletal ring vibrations of graphite. However, in the case of FePt/RGO, most of the peaks related to the oxygen functional groups including C=O, C-O, and O-H bands are absent, suggesting the reduction of GO into RGO. This result is consistent with XRD measurement. The band corresponding to the C-O groups at 1190 cm^{-1} still exists, because the C-O groups can't be totally removed by chemical reduction method [25]. The intense band located at 1565 cm^{-1} corresponds to the C=C stretching vibration, indicating the healing of the basal structure of the graphite domains.

Raman spectroscopy is a powerful technique to investigate order and disorder in the crystal structure of carbon [26-28]. Fig. 3 shows the typical Raman spectra of GO and

FePt/RGO. Two characteristic peaks at about 1330 cm^{-1} (D band, corresponding to κ-point phonons of A_{1g} symmetry) and 1590 cm^{-1} (G band, corresponding to an E_{2g} phonon of sp^2-bonded carbon atoms) are observed in the Raman spectra of GO and FePt/RGO. The intensity ratio of D band to G band (I_D/I_G), which is an indication of the extent π–conjugation and concentration of defects, are 0.95 and 1.10 for GO and FePt/RGO, respectively. This result suggests the electronic interactions between FePt nanoalloys and RGO sheets, thus benefiting electron transfer between them [29].

Fig. 4a and b show the representative TEM images of Pt/RGO and FePt/RGO nanocomposites, respectively. It is clearly shown that, Pt nanoparticles or FePt alloy nanoparticles are uniformly deposited on the RGO sheets. Most of the FePt and Pt nanoparticles is smaller than 10 nm, matching well with the results calculated with the Debye-Scherrer equation from (111) peak of the XRD pattern. The size distribution of FePt nanoparticles is more uniform than Pt. Most of the surface of RGO sheets is fully loaded with the FePt alloy nanoparticles. No free particles are observed outside the RGO sheets for both the two kinds of nanocomposites, suggesting the tight interaction between the RGO sheets and Pt/FePt nanoparticles, which are beneficial for rapid electron transfer between them.

Fig. 5a shows the SEM image of FePt/RGO nanocomposites. The nanocomposites exhibit typical wrinkled layer morphology of RGO sheets. The highly coarse surface of RGO sheets is densely covered with tiny FePt alloy nanoparticles. The corresponding EDS elemental mapping images of Pt (Fig. 5b) and Fe (Fig. 5c) further confirm the uniform and dense dispersion of FePt alloy nanoparticles on the surface of RGO sheets.

It can be clearly observed that, the RGO sheets are almost fully enveloped with the FePt alloy nanoparticles to form a sandwich-like composite structure. It is consistent with the TEM result. Moreover, the Pt and Fe elements are accompanied with each other in the elemental mapping images, indicating the successfully formation of FePt nanoalloys. The chemical composition of FePt/RGO nanocomposites is measured using EDS technique (Fig. 5d), which reveals the presence of respective elements of Fe, Pt, C, and O. The elements of Fe, Pt, and C should be ascribed to FePt/RGO nanocomposites. The small amount of O can be ascribed to the residual oxygen-containing functional groups of RGO, which agrees well with the existing C-O groups at 1190 cm^{-1} in the FTIR spectrum of FePt/RGO. As shown in the inset table of Fig. 5d, the weight ratio of Fe : Pt : C is measured to be 2.50 : 27.32 : 55.83 with the corresponding atomic ratio of 0.78 : 2.44 : 81.13 according to the EDS results. And the content of Pt in Pt/RGO nanocomposites is measured to be ~29% according to EDS analysis.

3.2 Electrochemical properties

The electrochemical behavior of the Pt/RGO nanocomposites and FePt/RGO nanocomposites is investigated using cyclic voltammograms (CV) at a scan rate of 50 mV s^{-1} in N_2-saturated 0.5 M H_2SO_4 solution. From Fig. 6, the voltammetric features of Pt/RGO and FePt/RGO are similar and show characteristic curves of polycrystalline Pt electrode, indicating the formation of the Pt skin on the alloy nanoparticles surface after electrochemical activation in 0.5 M H_2SO_4 [30]. For instance, for FePt/RGO electrode, a typical pair of broad current peaks related to the hydrogen adsorption-desorption can

be observed between +0.01 and -0.2 V. During the anodic scan, the Pt oxides are formed at the potential of above 0.5 V. And the reduction peak is located at 0.24 V in the cathodic sweep, which can be attributed to the reduction of Pt oxides. It is worth noting that, the peak currents of FePt/RGO electrode, including the reduction of Pt oxides and hydrogen adsorption-desorption, become more prominent compared with those of Pt/RGO electrode, suggesting a larger Pt skin layer on the particle surface.

The FePt/RGO catalyst is further employed in the subsequent electrooxidation of FA and methanol, revealing its enhanced electrocatalytic activity than Pt/RGO. Fig. 7a shows the CV curves of Pt/RGO and FePt/RGO in FA. It is well known that, the electrooxidation of FA on Pt could follow the so-called dual pathways mechanism [31-33]. One is a direct pathway involving the oxidation of FA into CO_2 at low potential. The other is an indirect pathway involving the production of poisoning CO intermediate and the further oxidation of CO to CO_2 at higher potential. As shown in Fig. 7a, only one peak at ~0.71 V (J_{a2}), which corresponds to the oxidation of CO generated by dehydration of HCOOH, is observed for Pt/RGO catalyst during the positive scan of the CV curve [33]. The oxidation current peak for direct oxidation of FA into CO_2 (J_{a1}) is absent, presenting a substantial proof of indirect electrocatalytic oxidation of FA on Pt/RGO catalyst. During the reversal scan, a peak corresponding to the direct oxidation of FA into CO_2 (J_c) with the catalyst surface free of CO poisoning is observed at ~0.41 V [30,33-35]. In comparison with it, the CV curve of FePt/RGO catalyst shows different features. It can be clearly seen in the inset of Fig. 7a, a new peak (J_{a1}) at ~0.3 V corresponding to the direct oxidation of FA into CO_2 is observed, indicating that the

FePt alloy nanoparticles exhibit enhanced catalytic activity than pure Pt nanoparticles. The current densities at J_{a2} and J_c of FePt/RGO increase dramatically compared with Pt/RGO. And during the negative scan, the onset and peak potential of FePt/RGO is positive than Pt/RGO, which reveals that FePt alloy nanoparticles possess higher catalytic activity on FA oxidation than Pt nanoparticles. Moreover, the J_{a1} is attributed to the direct FA oxidation and the J_c is assigned to the FA oxidation on the catalyst surface free of CO poisoning. So the J_{a1}/J_c ratio can essentially reflect the fraction of the catalysts surface that is not poisoned by CO adsorption, and can be used to measure the catalyst tolerance ability to CO poisoning [30]. For Pt/RGO, the absence of J_{a1} peak implies the serious poisoning of the catalyst surface by absorbed CO. On the other hand, the J_{a1}/J_c ratio for FePt/RGO is 0.26, which means that initially about 74% of the catalyst surface is poisoned by CO absorption, indicating the enhanced catalytic tolerance to CO. It is due to the fact that, the addition of Fe in FePt bimetallic alloy electroctalysts can maximize the absorption of FA on the Pt active sites as well as supply enough surface sites of the second metals to promote the effective oxidative removal of poisonous CO with adsorbed hydroxyl species [30,36].

In case of methanol oxidation, FePt/RGO catalyst also shows higher catalytic activity than Pt/RGO (Fig. 7b). It is generally accepted that, there are two peaks on the CV curve of methanol oxidation on Pt. As shown in Fig. 7b, the peak at the positive scan (I_f) corresponds to the electrooxidation of methanol, forming Pt adsorbed carbonaceous intermediates (mainly as CO). The peak located at the negative scan (I_b) is assigned to the oxidation of the absorbed intermediates generated via incomplete oxidation of

methanol during the positive scan. It can be clearly seen that, the peak currents of I_f and I_b for FePt/RGO are higher than that of Pt/RGO, and the onset potential of I_f peak for FePt/RGO is more negative, implying the superior catalytic activity of FePt/RGO on methanol oxidation. The I_f/I_b ratio is often employed to estimate the catalyst tolerance to CO [14,18]. FePt/RGO catalyst delivers higher value of 2.26 than 1.75 of Pt/RGO, indicating its better tolerance to CO poisoning, which is consistent with the result obtained from FA oxidation.

The catalytic activity and durability of Pt/RGO and FePt/RGO nanocomposites for FA/methanol oxidation are evaluated by choronoamperometrc measurements, respectively. Fig. 8a shows the *i-t* current curves of Pt/RGO and FePt/RGO on oxidation of FA. The currents of the two catalysts exhibit a fade and then reach steady values after several seconds, but the current of FePt/RGO fades slowly. The steady current density of FePt/RGO is 8.9 mA mg^{-1}, which is much higher than that of Pt/RGO (3.5 mA mg^{-1}), suggesting its superior catalytic stability. In Fig. 8b, the current of FePt/RGO on oxidation of methanol shows slighter decay than that of Pt/RGO. At 600 s, FePt/RGO delivers a higher current density of 8.1 mA mg^{-1} than 3.1 mA mg^{-1} for Pt/RGO, further confirming its enhanced catalytic activity and durability.

4. Conclusions

In summary, a novel two-step approach for the construction of FePt/RGO nanocomposites has been presented. The FePt nanoalloys are successfully formed and anchored on the surface of RGO sheets densely and uniformly. And the tight interaction

between the Pt/FePt nanoalloys and RGO sheets is beneficial for the electron transport. Aided with the introduction of Fe, the FePt/RGO catalyst exhibits higher electrocatalytic activity on FA/methanol oxidation, better tolerance to CO, and superior catalytic stability than Pt/RGO, thus making it a promising candidate as an efficient electrocatalyst in fuel cells. Furthermore, the presented FePt/RGO may find its potential applications in cell imaging, sensors, and drug delivery.

Acknowledgements

This work is financially supported by the National Natural Science Foundation of China (21003079), Research Award Fund for Outstanding Middle-Aged and Young Scientist of Shandong Province (BS2011CL020), Natural Science Foundation of Shandong Province (ZR2011BM018) and Qingdao Project of Science (12-1-4-3-(20)-jch).

References

[1] A.K. Geim, K.S. Novoselov, The rise of graphene, Nat. Mater. 6 (2007) 183-191.

[2] H. Zhang, M. Jin, Y. Xia, Enhancing the catalytic and electrocatalytic properties of Pt-based catalysts by forming bimetallic nanocrystals with Pd, Chem. Soc. Rev. 41 (2012) 8035-8049.

[3] J. Wu, H. Yang, Platinum-based oxygen reduction electrocatalysts, Acc. Chem. Res. 46 (2013) 1848-1857.

[4] X. Zhou, Y. Gan, J. Du, D. Tian, R. Zhang, C. Yang, Z. Dai, A review of hollow Pt-based nanocatalysts applied in proton exchange membrane fuel cells, J. Power

Sources 232 (2013) 310-322.

[5] P. Yu, M. Pemberton, P. Plasse, PtCo/C cathode catalyst for improved durability in PEMFCs, J. Power Sources 144 (2005) 11-20.

[6] V. Stamenkovic, B.S. Mun, K.J.J. Mayrhofer, P.N. Ross, N.M. Markovic, J. Rossmeisl, J. Greeley, J.K. Nørskov, Changing the activity of electrocatalysts for oxygen reduction by tuning the surface electronic structure, Angew. Chem., Int. Ed., 45 (2006) 2897-2901.

[7] V.R. Stamenkovic, B.S. Mun, M. Arenz, K.J.J. Mayrhofer, C.A. Lucas, G. Wang, P.N. Ross, N.M. Markovic, Trends in electrocatalysis on extended and nanoscale Pt-bimetallic alloy surfaces, Nat. Mater. 6 (2007) 241-247.

[8] J. Wang, R.M. Asmussen, B. Adams, D.F. Thomas, A. Chen, Facile synthesis and electrochemical properties of intermetallic PtPb nanodendrites, Chem. Mater. 21 (2009) 1716-1724.

[9] A. Miura, H. Wang, B.M. Leonard, H.D. Abruña, F.J. DiSalvo, Synthesis of intermetallic PtZn nanoparticles by reaction of Pt nanoparticles with Zn vapor and their application as fuel cell catalysts, Chem. Mater. 21 (2009) 2661-2667.

[10] Y. Bing, H. Liu, L. Zhang, D. Ghosh, J. Zhang, Nanostructured Pt-alloy electrocatalysts for PEM fuel cell oxygen reduction reaction, Chem. Soc. Rev. 39 (2010) 2184-2202.

[11] D. Xu, S. Bliznakov, Z. Liu, J. Fang, N. Dimitrov, Composition-dependent electrocatalytic activity of Pt-Cu nanocube catalysts for formic acid oxidation, Angew. Chem., Int. Ed. 49 (2010) 1282-1285.

[12] W. Yu, M.D. Porosoff, J.G. Chen, Review of Pt-based bimetallic catalysis: from model surfaces to supported catalysts, Chem. Rev. 112 (2012) 5780-5817.

[13] S. Guo, S. Sun, FePt nanoparticles assembled on graphene as enhanced catalyst for oxygen reduction reaction, J. Am. Chem. Soc. 134 (2012) 2492-2495.

[14] G. Wei, Y. Zhang, S. Steckbeck, Z. Su, Z. Li, Biomimetic graphene–FePt nanohybrids with high solubility, ferromagnetism, fluorescence, and enhanced electrocatalytic activity, J. Mater. Chem. 22 (2012) 17190-17195.

[15] T. Ghosh, Q. Zhou, J.M. Gregoire, R.B. van Dover, F.J. DiSalvo, Pt– Cd and Pt–Hg phases as high activity catalysts for methanol and formic acid oxidation, J. Phys. Chem. C 114 (2010) 12545-12553.

[16] B. Habibi, N. Delnavaz, Electrosynthesis, characterization and electrocatalytic properties of Pt–Sn/CCE towards oxidation of formic acid, RSC Adv. 2 (2012) 1609-1617.

[17] Y. Kang, L. Qi, M. Li, R.E. Diaz, D. Su, R.R. Adzic, E. Stach, J. Li, C.B. Murray, highly active Pt_3Pb and core–shell Pt_3Pb–Pt electrocatalysts for formic acid oxidation, ACS Nano 6 (2012) 2818-2825.

[18] Z. Ji, G. Zhu, X. Shen, H. Zhou, C. Wu, M. Wang, Reduced graphene oxide supported FePt alloy nanoparticles with high electrocatalytic performance for methanol oxidation, New J. Chem. 36 (2012) 1774-1780.

[19] X. Zhao, J. Zhu, W. Cai, M. Xiao, L. Liang, C. Liu, W. Xing, Pt–Pb hollow sphere networks: self-sacrifice-templating method and enhanced activity for formic acid electrooxidation, RSC Adv. 3 (2013) 1763-1767.

[20] H. Bai, C. Li, G. Shi, Functional composite materials based on chemically converted graphene, Adv. Mater. 23 (2011) 1089-1115.

[21] N.G. Sahoo, Y. Pan, L. Li, S.H. Chan, Graphene‐Based Materials for Energy Conversion, Adv. Mater. 24 (2012) 4203-4210.

[22] J. Guo, B. Jiang, X. Zhang, X. Zhou, W. Hou, $Fe_{2.25}W_{0.75}O_4$/reduced graphene oxide nanocomposites for novel bifunctional photocatalyst: One-pot synthesis, magnetically recyclable and enhanced photocatalytic property, J. Solid State Chem. 205 (2013) 171-176.

[23] Y. Si, E.T. Samulski, Exfoliated graphene separated by platinum nanoparticles, Chem. Mater. 20 (2008) 6792-6797.

[24] S. Yang, W. Yue, J. Zhu, Y. Ren, X. Yang, Graphene-based mesoporous SnO_2 with enhanced electrochemical performance for lithium-ion batteries, Adv. Funct. Mater. 23 (2013) 3570-3576.

[25] D. Li, M.B. Müller, S. Gilje, R.B. Kaner, G.G. Wallace, Processable aqueous dispersions of graphene nanosheets, Nat. Nanotechnol. 3 (2008) 101-105.

[26] R.I. Jafri, N. Rajalakshmi, S. Ramaprabhu, Nitrogen doped graphene nanoplatelets as catalyst support for oxygen reduction reaction in proton exchange membrane fuel cell, J. Mater. Chem. 20 (2010) 7114-7117.

[27] M. Zhang, B. Qu, D. Lei, Y. Chen, X. Yu, L. Chen, Q. Li, Y. Wang and T. Wang, A green and fast strategy for the scalable synthesis of Fe_2O_3/graphene with significantly enhanced Li-ion storage properties, J. Mater. Chem. 22 (2012) 3868-3874.

[28] Z. Lin, G. Waller, Y. Liu, M. Liu, C.P. Wong, Facile synthesis of nitrogen-doped graphene via pyrolysis of graphene oxide and urea, and its electrocatalytic activity toward the oxygen-reduction reaction, Adv. Energy Mater. 2 (2012) 884-888.

[29] C. Xu, J. Sun, L. Gao, Direct growth of monodisperse SnO_2 nanorods on graphene as high capacity anode materials for lithium ion batteries, J. Mater. Chem. 22 (2012) 975-979.

[30] W. Chen, J. Kim, S. Sun, S. Chen, Composition effects of FePt alloy nanoparticles on the electro-oxidation of formic acid, Langmuir 23 (2007) 11303-11310.

[31] G.R. Zhang, D. Zhao, Y.Y. Feng, B. Zhang, D.S. Su, G. Liu, B.Q. Xu, Catalytic Pt-on-Au nanostructures: why Pt becomes more active on smaller Au particles, ACS Nano 6 (2012) 2226-2236.

[32] R. Iyyamperumal, L. Zhang, G. Henkelman, R.M. Crooks, Efficient electrocatalytic oxidation of formic acid using Au@ Pt dendrimer-encapsulated nanoparticles, J. Am. Chem. Soc. 135 (2013) 5521-5524.

[33] A. Capon, R. Parsons, The oxidation of formic acid at noble metal electrodes: I. Review of previous work, J. Electroanal. Chem. 44 (1973) 1-7.

[34] N. Kristian, Y. Yan, X. Wang, Highly efficient submonolayer Pt-decorated Au nano-catalysts for formic acid oxidation, Chem. Commun. (2008) 353-355.

[35] J.B. Xu, T.S. Zhao, Z.X. Liang, Synthesis of active platinum−silver alloy electrocatalyst toward the formic acid oxidation reaction, J. Phys. Chem. C 112 (2008) 17362-17367.

[36] N. Tian, Z.Y. Zhou, S.G. Sun, Y. Ding, Z.L. Wang, Synthesis of tetrahexahedral

platinum nanocrystals with high-index facets and high electro-oxidation activity, Science 316 (2007) 732-735.

Figure captions:

Fig. 1. (a) XRD patterns of GO, Pt/RGO nanocomposites and FePt/RGO nanocomposites; (b) the magnified XRD (111) peaks of Pt/RGO nanocomposites and FePt/RGO nanocomposites.

Fig. 2. FTIR spectra of GO and FePt/RGO nanocomposites.

Fig. 3. Raman spectra of GO and FePt/RGO nanocomposites.

Fig. 4. TEM images of (a) Pt/RGO nanocomposites and (b) FePt/RGO nanocomposites.

Fig. 5. SEM image (a) and the corresponding EDS elemental mapping images of (b) Pt, (c) Fe. (d) EDS spectrum of FePt/RGO nanocomposites. The inset shows the atomic and weight ratio of Fe, Pt, and C elements in the FePt/RGO nanocomposites.

Fig. 6. CV curves of Pt/RGO and FePt/RGO nanocomposites in 0.5 M H_2SO_4 solution.

Fig. 7. CV curves of Pt/RGO and FePt/RGO nanocomposites in 0.5 M H_2SO_4 solution containing (a) 1 M HCOOH and (b) 0.5 M CH_3OH at a scan rate of 50 mV s^{-1}. Inset in (a) shows the enlarged CV curves of electrooxidation of HCOOH between -0.2~0.6 V during the positive scan.

Fig. 8. Choronoamperometrc curves of Pt/RGO and FePt/RGO nanocomposites in 0.5 M H_2SO_4 solution containing (a) 1 M HCOOH and (b) 0.5 M CH_3OH.

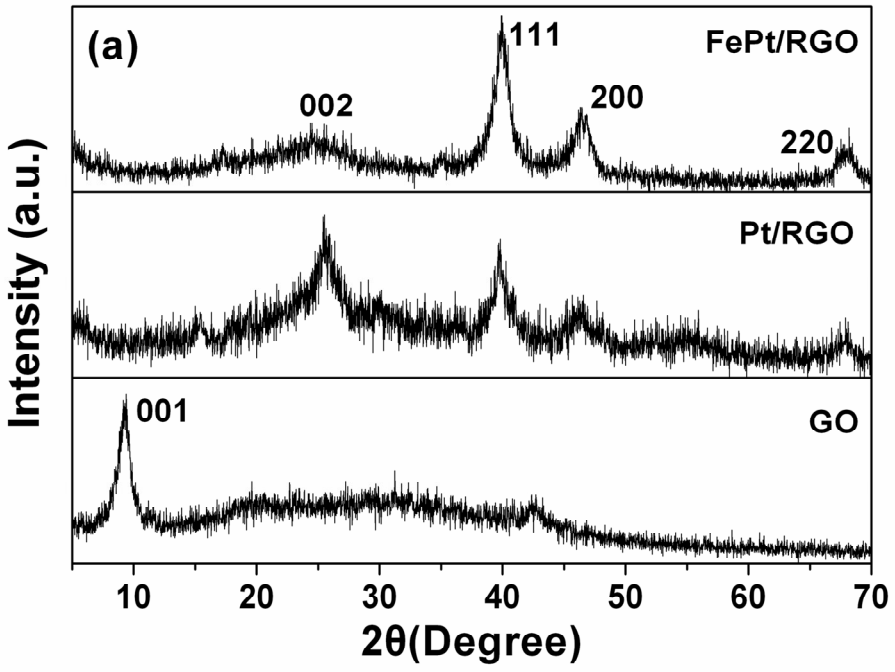

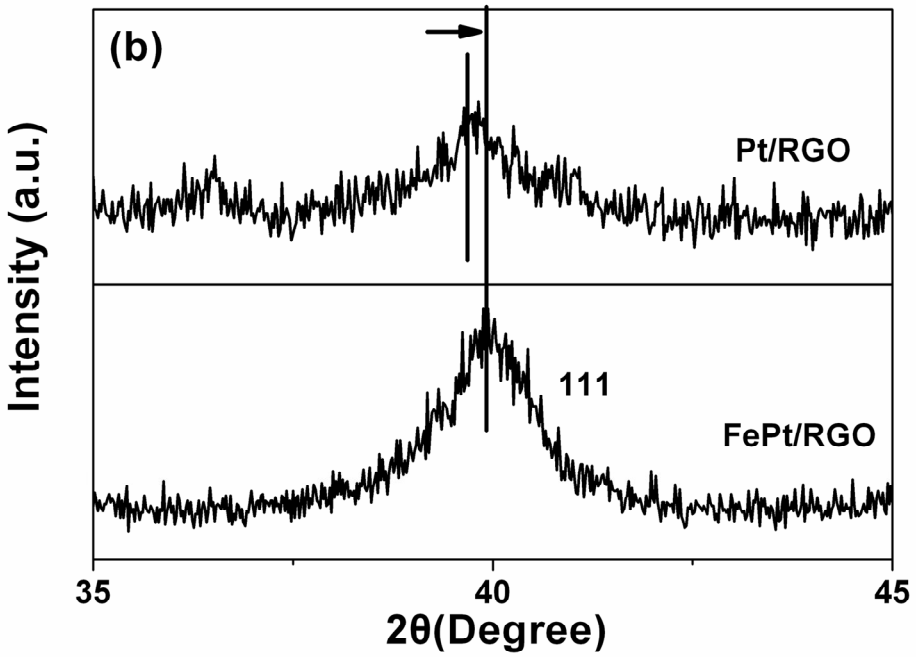

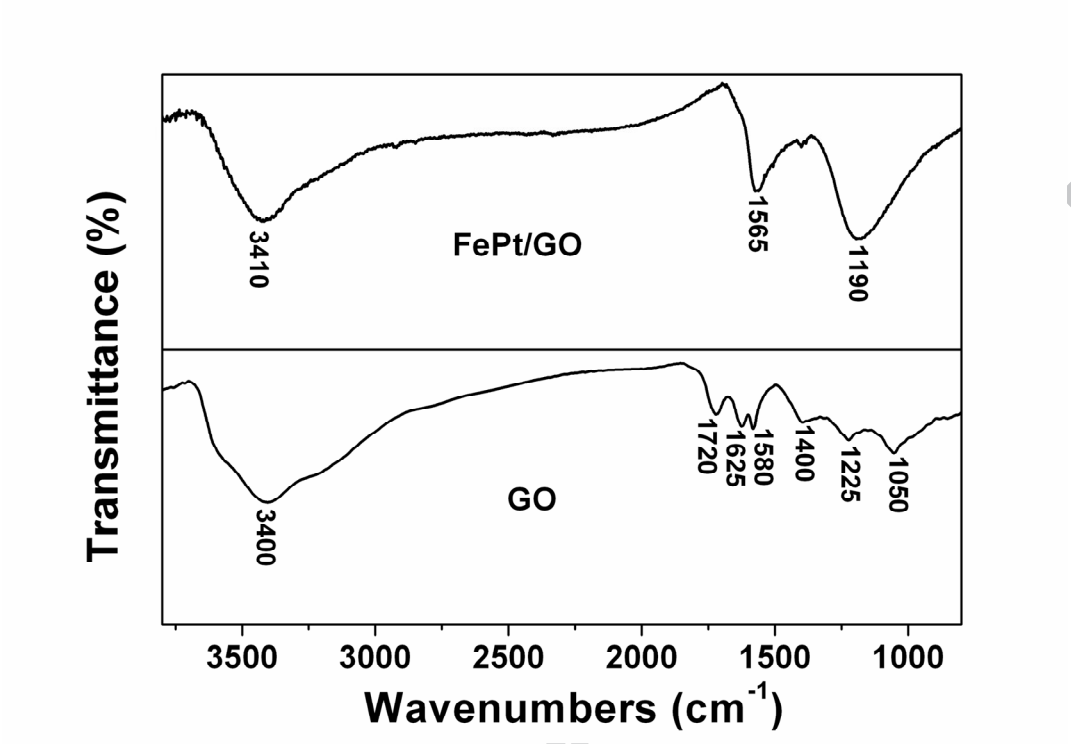

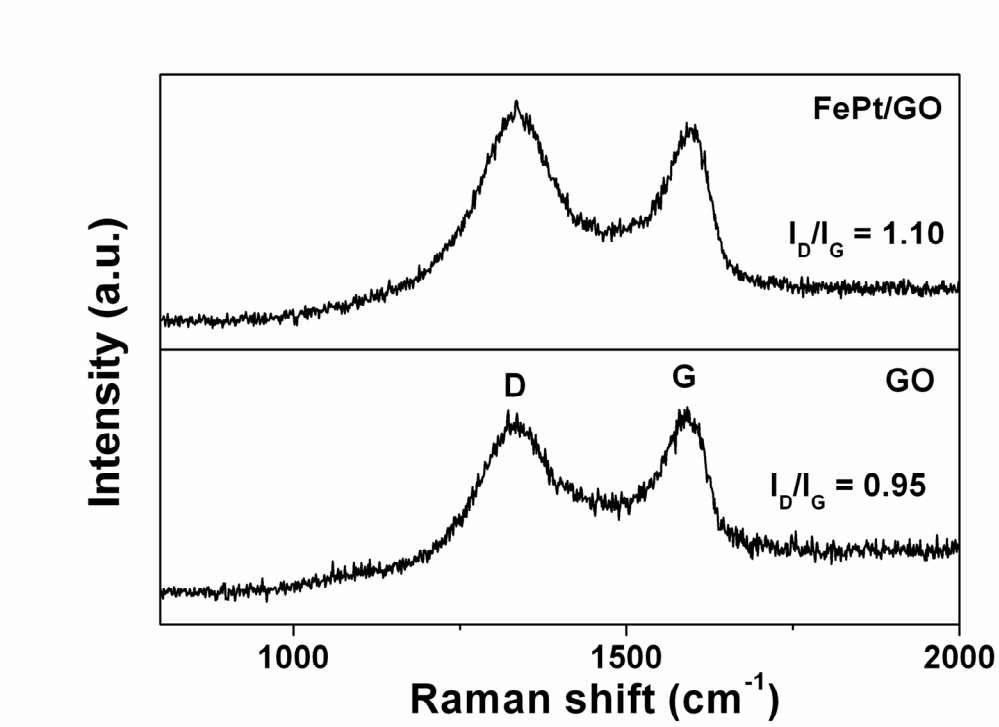

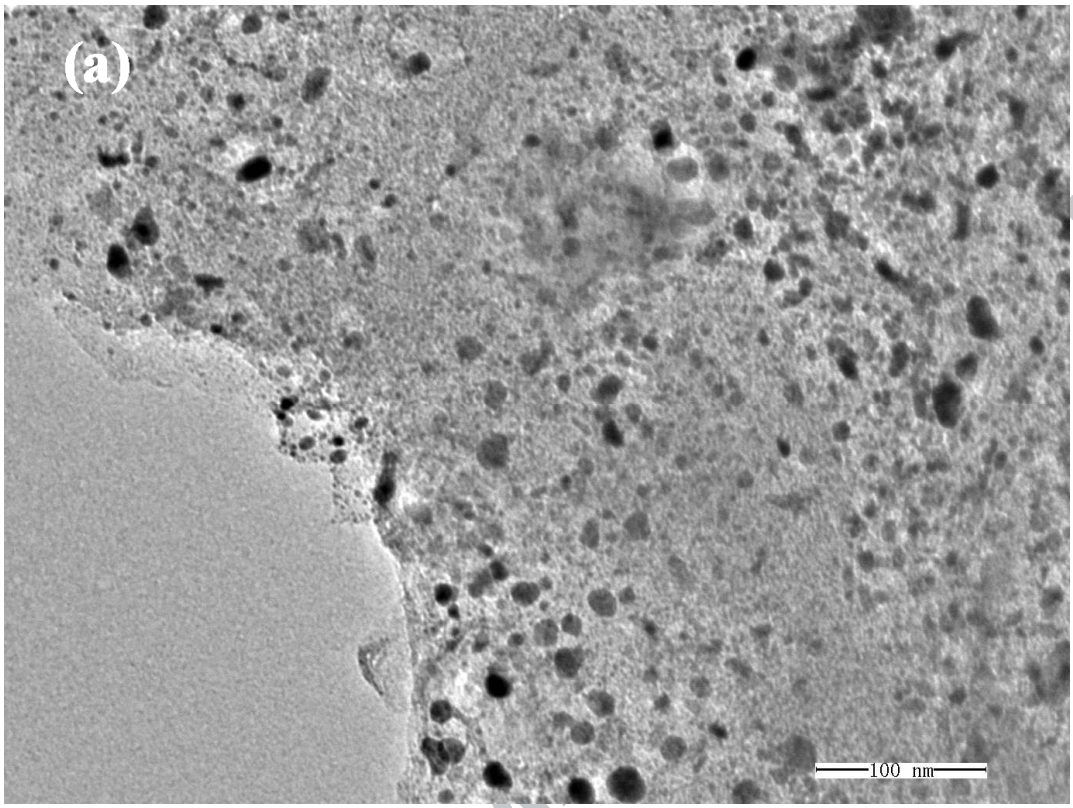

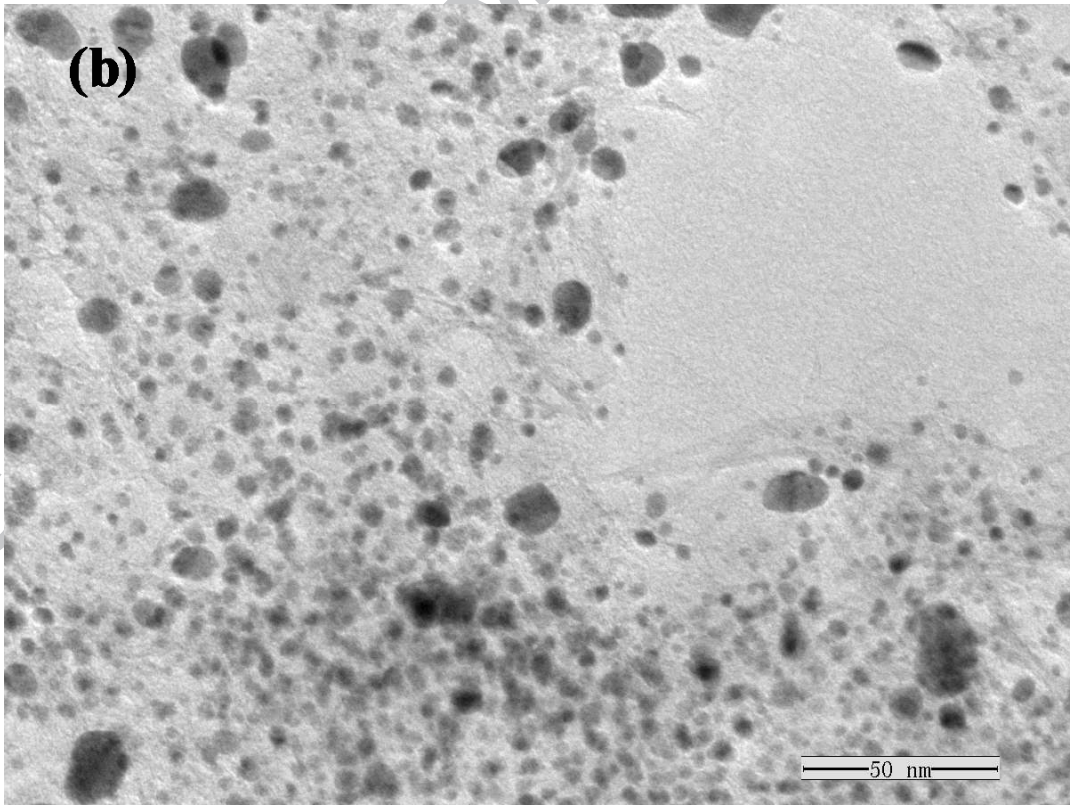

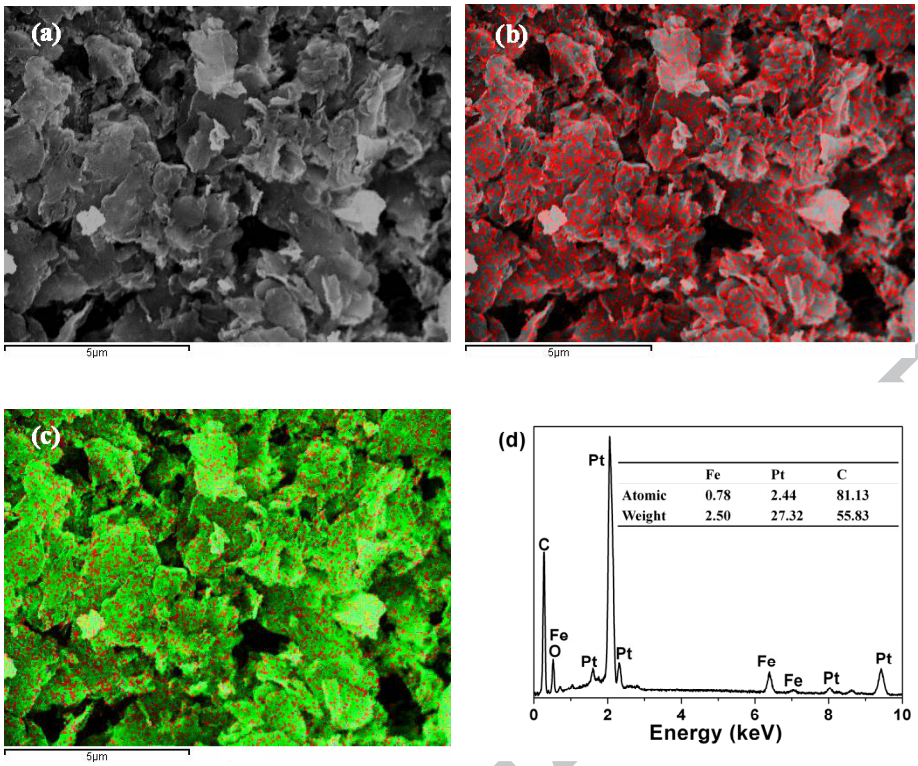

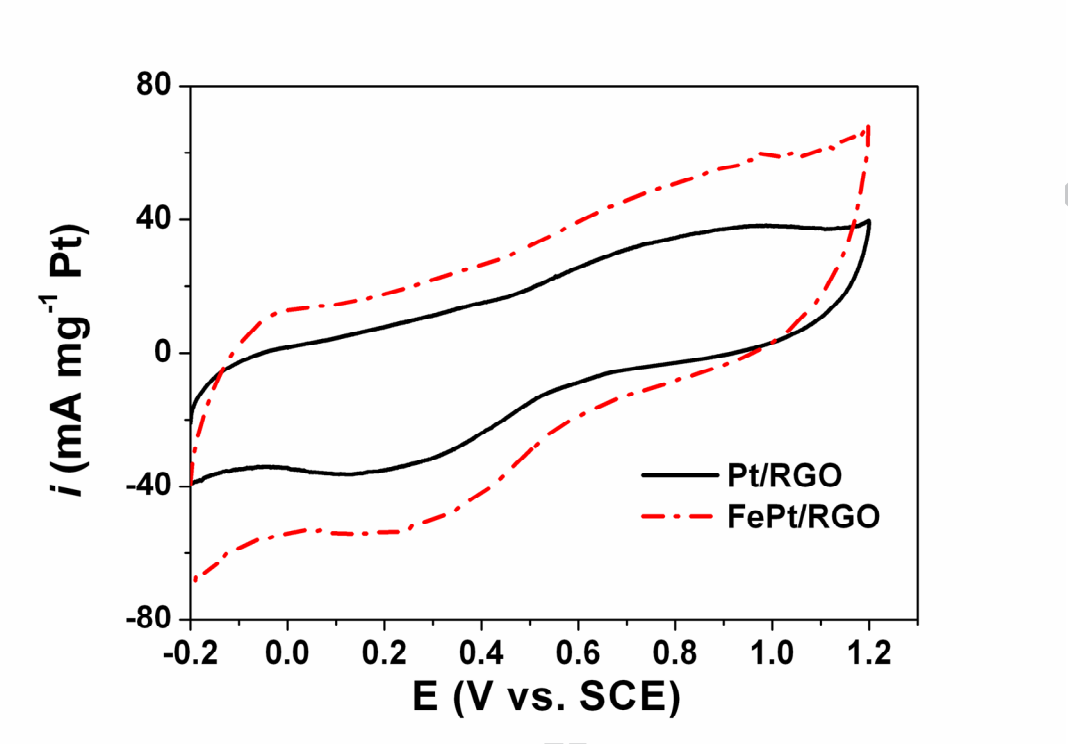

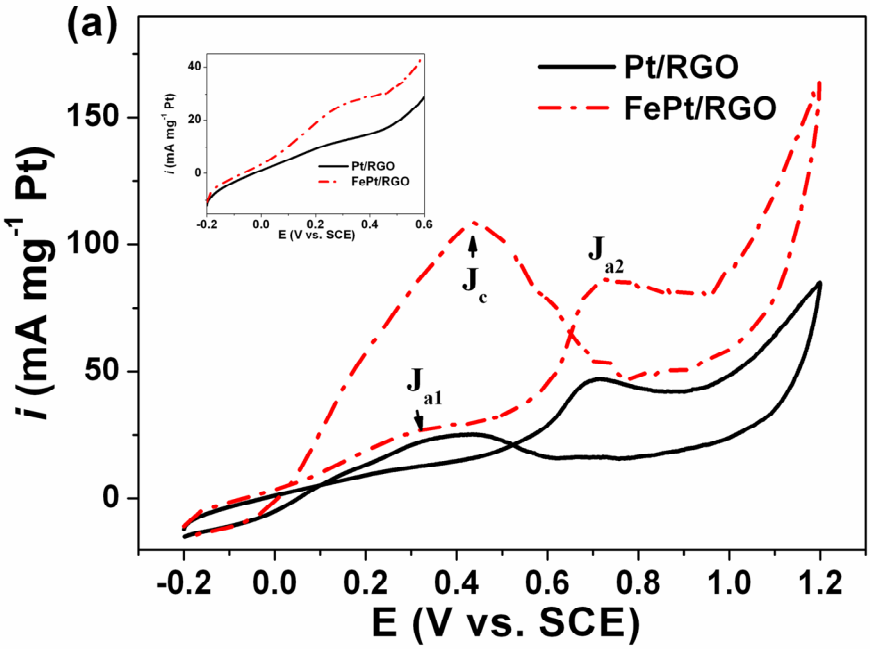

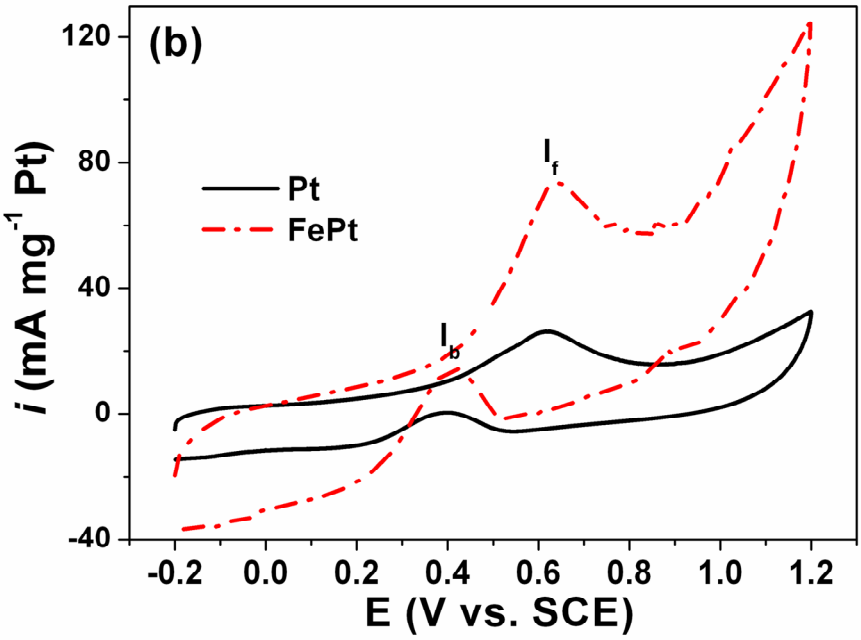

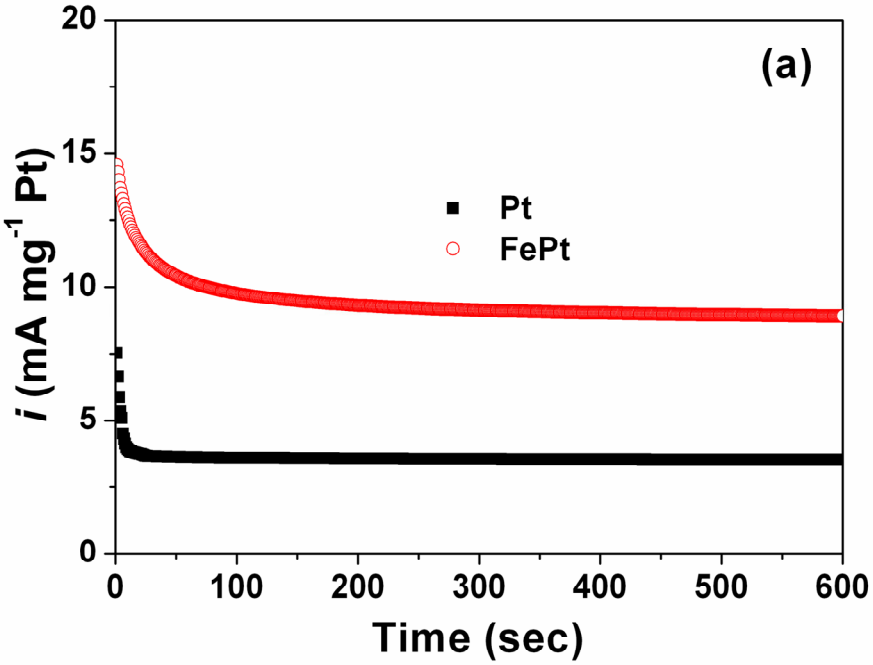

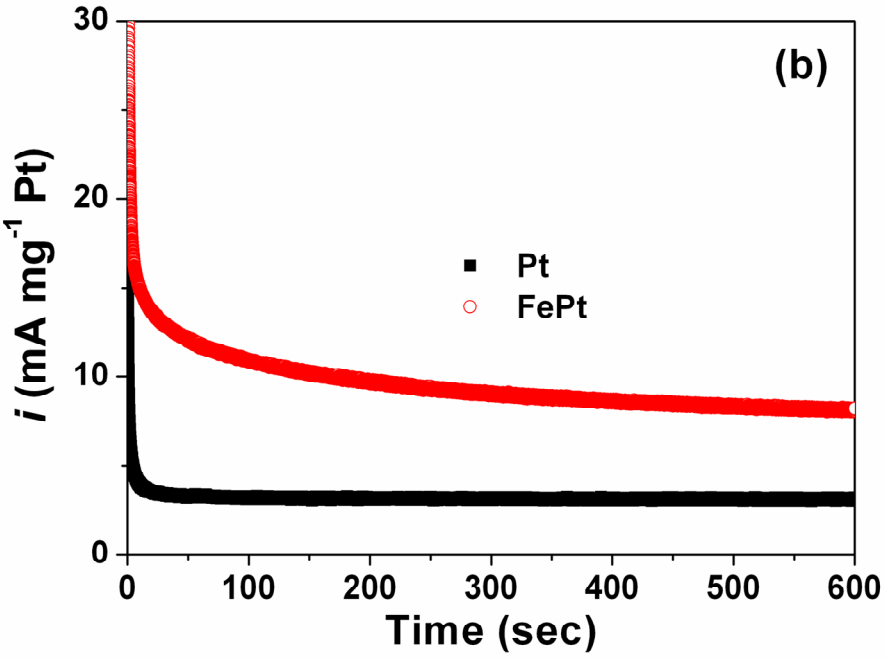

FePt alloy nanoparticles anchored RGO composites are successfully synthesized.

The alloying of Fe with Pt is demonstrated with XRD and elemental maps.

FePt/RGO show enhanced catalytic activity on FA/methanol oxidation than Pt/RGO.

FePt/RGO also exhibit improved tolerance to CO poisoning than Pt/RGO.